MARY KAY O'CONNOR PROCESS SAFETY CENTER
TEXAS A&M ENGINEERING EXPERIMENT STATION

19th Annual International Symposium
October 25-27, 2016 • College Station, Texas

A Medium-Scale Cryogenic Spill Study to Estimate Vapor Formation on Concrete Substrate

Monir Ahammad[1*], *Syed Quraishy*[2], *Tomasz Olewski*[2], *Sam Mannan*[1] *and Luc Véchot*[2,]

[1]*Mary Kay O'Connor Process Safety Center, Texas A&M University, College Station, Texas, USA*

[2]*Mary Kay O'Connor Process Safety Center Extension at Qatar, Texas A&M University at Qatar, Doha, Qatar.*

**Presenter Email: monir@tamu.edu*

Abstract

This paper presents the findings of medium-scale (5 - 15 kg) cryogenic liquid experiments on a concrete substrate which may represent an industrial grade diking material. The temperature varying thermal characteristics, *i.e.* the conductivity (*k*) and heat capacity (*Cp*) of the concrete substrate were measured in the range of -160°C to 50°C using guarded hot plate and DSC, respectively. Vaporization rate of liquid nitrogen (LN_2), liquid oxygen (LO_2) and a mixture of 80% LN_2 and 20% LO_2, (*i.e.* liquid air) were studied on the same concrete substrate. It was found that conductive heat transfer from the concrete substrate has the greatest contribution in the vaporization of cryogenic liquids. The evidence of phase change from film boiling to nucleate boiling was observed during the pool vaporization of LO_2. The effect of preferential boiling on the temperature and heat flux profiles inside the concrete substrate was also observed. The change of heat fluxes due to the preferential boiling after each refill of mixture liquids were found to vary from 3% to 15%. Finally, the recorded heat flux during the early and later stages of pool vaporization were 12.4 kW/m^2 and 3.7 kW/m^2 for LN_2 and 12.9 kW/m^2 and 2.96 kW/m^2 for LO_2.

Keywords: Cryogenic spill, source-term, vaporization on concrete, preferential boiling, phase change

1. Introduction

In case of an accidental spill of cryogenic liquids, vapor will form due to the heat transferred from substrates (conductive), atmosphere (convective) and (/or) from radiation sources (*e.g.* sun, fire). Different cryogenic materials may cause similar or different types of hazardous situations, owing to the nature of formed vapor cloud. For example, liquefied natural gas (LNG) vapor cloud may cause many hazardous situations, such as – (a) an asphyxiating environment when the cloud stays closer to the ground at low temperature, (b) An early ignition of LNG vapor may result in flash fire and/or pool fire, (c) a late ignition may increase the severity of the event by causing a vapor cloud explosion in a highly congested space. A LN_2 vapor cloud may result in an asphyxiating environment. An individual exposed to such conditions may suffer from non-reversible health condition when the oxygen concentration goes below 19.5% [1]. LO_2 and its vapor are very reactive and help violently burning or oxidizing flammable and combustible materials. An oxygen enriched atmosphere beyond 23.5% is also dangerous according to OSHA confined space entrance standard (1910.146).

Industrial standards such as NFPA 59A [2] specified the use of dikes or impoundment area around the LNG containers to prevent uncontrolled dispersion of LNG and its vapor. The most common dikes floor material is concrete. If LNG containment tank fails, the cryogenic liquid will boil up due to heat transferred from dike floors and the walls. The severity of a spill event would depend on the size of the vapor cloud. Therefore, it is important to study the vaporization rate, more frequently referred as vaporization "source-term", to accurately predict the risk in the cryogenic processing facility.

Experimental study suggests that conductive heat transfer from the solid substrate to the liquid pool is the main mode of heat transfer during pool vaporization. Some argues whether conductive heat transfer is the dominant mode throughout the pool vaporization period [11]. Other studies suggest, convection and solar radiation can be accounted for less 5% of the total mass vaporization [5–7]. Despite, it is well accepted that conduction heat transfer from the substrate is the major heat transfer source in cryogenic pool vaporization, at least in the beginning of the spill, if not during entire vaporization period [3]. Briscoe and Shaw developed a model based on the assumption that the conductive heat transfer from the ground is the dominant heat transfer mechanism [4]. A proper use of such model requires the thermo-physical characteristics of the ground material [8]. A theoretical vaporization models, whether simple as 1-D Briscoe & Shaw model or advanced as CFD study by [9], experimental investigations are still necessary to validate the aforementioned theoretical models.

Understanding the importance of LNG vaporization "source-term" in determining the severity of loss of primary containment, Reid and Wang [10] have studied this parameter for LNG on insulated dike floors. In their study, pure methane was considered as LNG. As a result, the effect of mixture boiling on vaporization rate was left uninvestigated. Moreover, an insulated floor might not be a realistic case an industrial setting. Thus, further study of the cryogenic source-term on a non-insulated concrete ground is still an important area for research. The source-term investigation results will be helpful in determining a spill consequence severity and the risk of the processing facility.

A laboratory scale analysis of LN_2 vaporization due to different heat transfer mechanisms were conducted by Vechot et al [11] in a Dewar flask. They have reported that convective and radiative heat transfer plays a significant role in the vaporization of LN_2 particularly in the later stages of pool boiling. However, the limitation of their experiment is that in an actual spill scenario, the cryogenic liquid (*e.g.* LNG) may not be contained within insulated walls and floor. Rather the pool of liquid will boil due to the conductive heat transfer from the dike walls and floor along with other sources of heat such as convective and radiative heats. Another limitation of this study was a small amount of cryogenic liquid (~2 kg) was allowed to vaporize. Therefore, the results of this study may not be accurate, when extrapolated for a full scale industrial spill. Nevertheless it is worth mentioning that an industrial scale spill experiment is very expensive. Other small scale study of LN_2 vaporization on water and ice substrates were addressed by Gopalaswami *et al.*[12,13]. This study focuses on a medium scale field experiment (5-50 kg) on concrete substrate. The investigation findings are expected to improve the understanding of an actual spill scenario.

An early review of cryogenic spill data were conducted by Prince [14] and a recent one by Thyer [15]. Thyer has reviewed 39 cryogenic spill experiments reported in the literature. His analysis showed that seven of these experiments were too lacking in capturing detail information to be usable. A concrete substrate was used in 7 among the 32 hazardous material spill studies. Three among these seven studies were focused on hazardous materials such as chlorine, hydrogen, oxygen, and water. A deeper analysis of the remaining 4 studies revealed the type material hazardous material used was pure methane but referred as LNG. This might result in some prediction error as literature suggests that multicomponent mixtures may have a significant influence in vaporization [16]. Apart from that, three studied vaporization on insulated concrete floors. The remaining one study did not characterize the substrate concrete. Thus, it can be concluded that the vaporization characteristics of pure and mixture cryogens (*e.g.* LN_2, LO_2, LNG) on actual dike floor material (*i.e.* concrete) is lacking in the literature.

This study focuses on the vaporization of LN_2 and LO_2 on concrete substrates. Literature suggests that influence of multi-component mixtures can be significant for other cryogenic liquids such as LNG and LPG [16]. Therefore, to understand the influence of multi-component, a mixture of initial composition of 80% LN_2 and 20% LO_2 is also studied to capture the effect of preferential boiling during vaporization of mixtures. Thus, this study is expected to contribute in generating experimental knowledge of cryogenic vaporization source-term and will help the existing models in validating their assumptions. In this study, the liquid mass vaporization, temperature and heat flux profiles inside the substrates were investigated. Thermo-physical characteristics of concrete substrate were determined at different temperatures.

2. Experimental

A series of experiments were performed in a wind tunnel of Qatar Petroleum's fire station -2 at Ras Laffan Industrial City, Qatar. Experiments were performed in the period of April to May 2014. First day included the spill of liquid nitrogen (LN_2) only and was performed on April 22nd, 2014. Second experiment included the spill of liquid nitrogen and liquid oxygen mixture (LN_2-LO_2) and was performed on April 28th, 2014 and the third experiment included the spill of liquid oxygen (LO_2) only and was performed on May 13th, 2014.

2.1 Schematic Diagram of the Experimental Setup

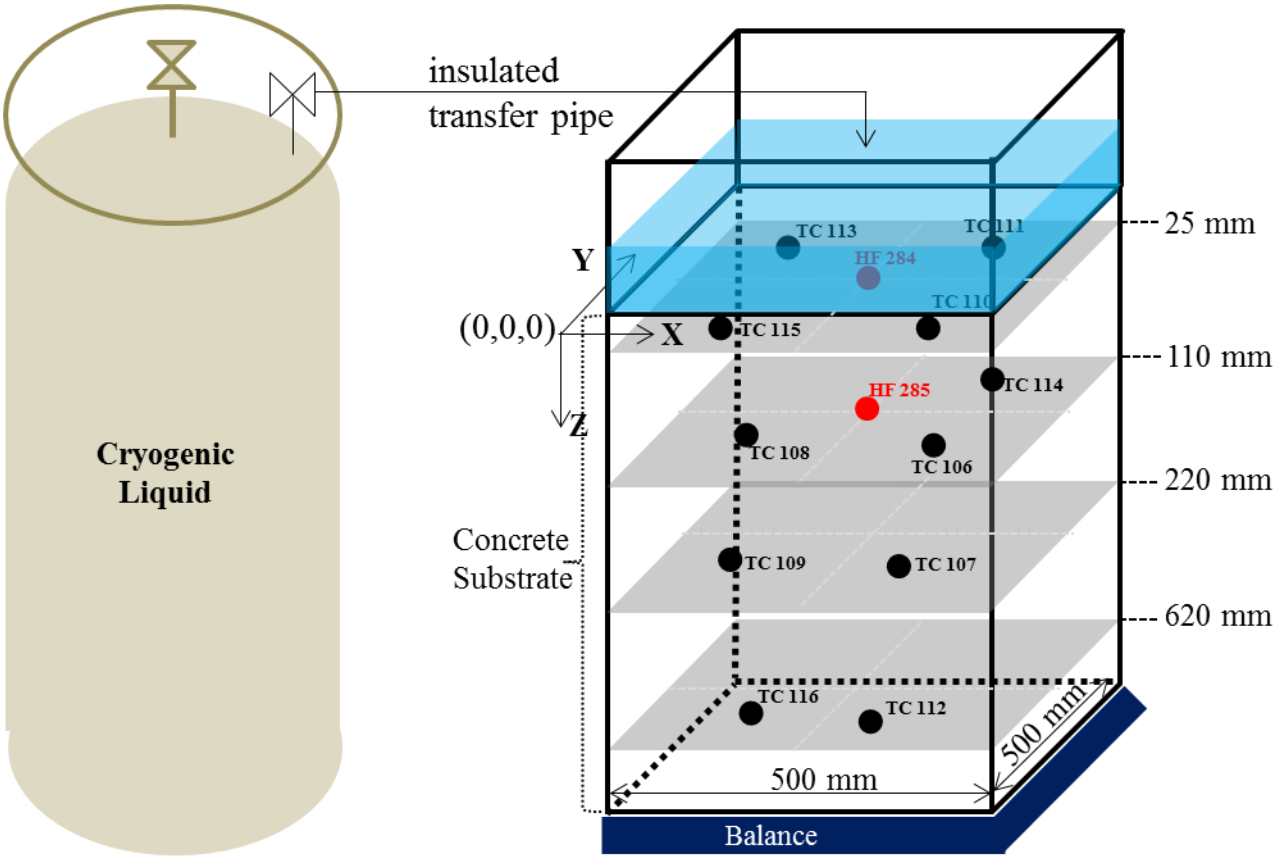

Figure 1 presents a schematic diagram of the experimental setup. Cryogenic liquid (i.e. LN_2, LO_2 and an initial mixture of 80% LN_2 and 20% LO_2) were poured in a box of concrete substrate. A 30 feet long connecting hose with a vapor and liquid separator at the open end is used to transfer the liquid from the cryogenic liquid tank to the experimental setup. To subside the vaporization of cryogens inside the liquid hose, it was insulated and was protected from the solar radiation. Steel plates were used to construct the liquid holding box of (500 mm x 500 mm x 300 mm) on the top of the concrete substrate. The dimension of the concrete substrate was 500 mm x 500 mm x 650 mm. The area of the substrate face in contact with

the liquid was 500 mm x 500 mm. The set-up was insulated at the outside using 3 inch polystyrene foams to reduce the heat transfer due to convective heating. The top of the liquid holding tank was also covered with insulating polystyrene to reduce the atmospheric convective heat transfer. Eleven thermocouples of type N with a sensitivity of ±0.01°C and two heat flux measuring sensor plates of Hukseflux, HF-01 type, with a sensitivity of ± 1084 μV/W/m^2, were placed in 4 layers inside the concrete substrate. The exact locations of the thermocouples (TC) and heat flux sensors (HF) were given in Table 1. TC-110, TC-111, TC-113, TC-115 thermocouples and HF-284 heat flux sensor were placed in the 1st layer beneath the boiling liquid at an approximate depth of 25 mm. In 2nd layer, TC-108, TC-114, TC-106 thermocouples and HF-285 heat flux sensor were placed at an approximate depth of 110 mm. In the 3rd layer, at the depth of 220 mm, TC-107, and TC-109 thermocouples were placed. Finally, in the 4th layer, at the depth of 620 mm, TC-112, TC-116 thermocouples were placed. It should be noted that the heat flux plate sensors measures both the temperature and the heat flux at its location. The overall setup was placed on a balance with a sensitivity of ±60gm. This whole instrumented set-up was connected to a data acquisition system.

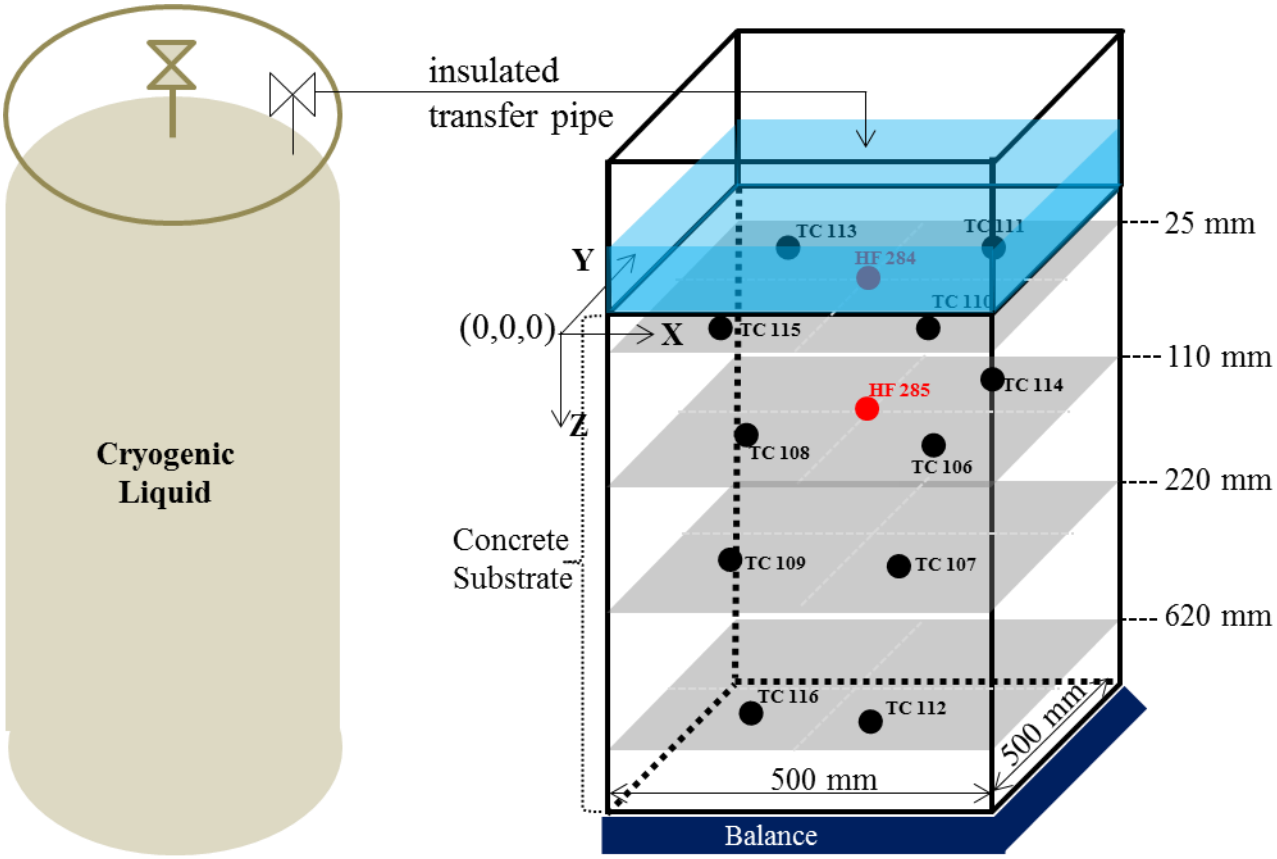

Figure 1: Schematic diagram of the experimental setup. Black dots represent the location of thermocouples inside concrete substrates and heat flux sensors location was indicated by the red dots.

Table 1: Coordinates of the thermocouple and heat flux sensors' locations inside the concrete substrate

	Layer 1				Layer 2		
	X (mm)	Y(mm)	Z(mm)		X (mm)	Y(mm)	Z(mm)
TC-110	248.8	117.5	28.5	**TC-106**	264	120.5	111
TC-111	320.5	273.5	24	**TC-108**	132.5	122.5	111

TC-113	72.3	278.8	33	**TC-114**	312.3	274	110.5
TC-115	132.8	121.8	25	**HF-T-285**	193	168.5	96.5
HF-T-285	197.5	168.5	28.5	**HF-X-285**	193	168.5	96.5
HF-X-284	197.5	168.5	28.5				
Layer 3				**Layer 4**			
	X (mm)	Y(mm)	Z(mm)		X (mm)	Y(mm)	Z(mm)
TC-107	265	115.3	226.5	**TC-112**	258.8	119.3	622
TC-109	128.8	119.5	220	**TC-116**	120	122	621.5

2.2 Thermo-Physical Properties of the Concrete Substrate

Industrial grade concrete that were used in the construction of Testing Prop-5 at Ras Laffan Emergency Safety College in Qatar were used to construct the concrete substrate of this experimental setup. The thermo-physical properties of the concrete composites were experimentally determined at NETZSCH Instruments Testing Laboratory, Burlington, MA, for various temperatures. Standard procedures (ASTM C 177-10, Steady-state heat flux measurements and thermal transmission properties by means of guarded hot plate apparatus, utilizing a Holometrix Model) were followed to measure the thermal conductivity. Two concrete slabs, of same composition to our experimental setup of dimensions 305 mm by 305 mm square with a thickness of 43 mm were used to test for thermal conductivity. The densities of the used samples were determined as 2335 kg/m^3. Figure 2 shows the dependency of thermal conductivity on the mean temperature between the top and bottom surfaces. The reported results have uncertainty of lower than 7%. It is observed that conductivity increases linearly between -161°C to -66°C. At higher temperature range, from -41°C to 50°C, the rate of increase is smaller than the lower temperature range. Between -66°C and -41°C, it was found that the rate of change of conductivity with mean temperature is negative.

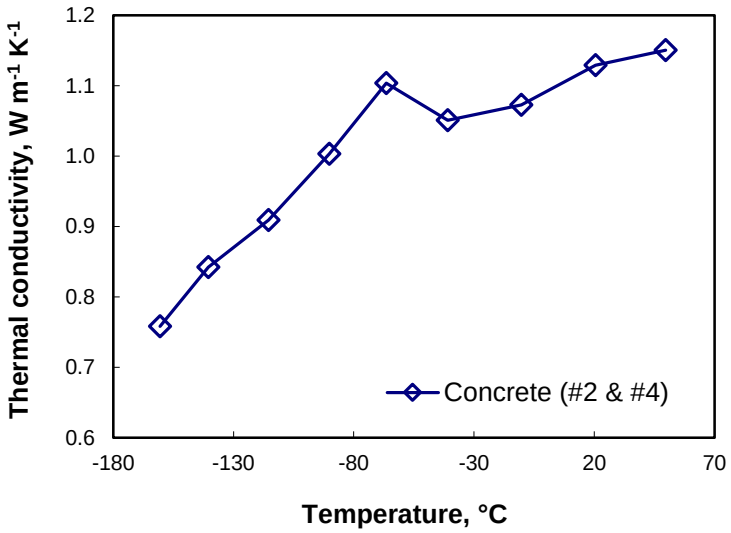

Figure 2: Thermal conductivity of the concrete as function of mean temperature

Furthermore, four small concrete samples, (i.e. sample 1 to 4), of 12.61 mg, 10.02 mg, 10.02 mg, and 10.54 mg were tested using a Differential Scanning Calorimeter (DSC) to determine the specific heat capacity (*Cp*). Figure 3 depicts the *Cp* as a function of temperature in the range of -160°C to 50°C. It is clear that the specific heat increases linearly with the increase of temperature. However, a variability of 0.046 J/gK among the four samples was observed at -160°C. At higher temperature, *Cp* has varied more comparing to lower temperatures. At 50°C, the *Cp* variability among the four tested samples was reported as 0.122 J/g.K.

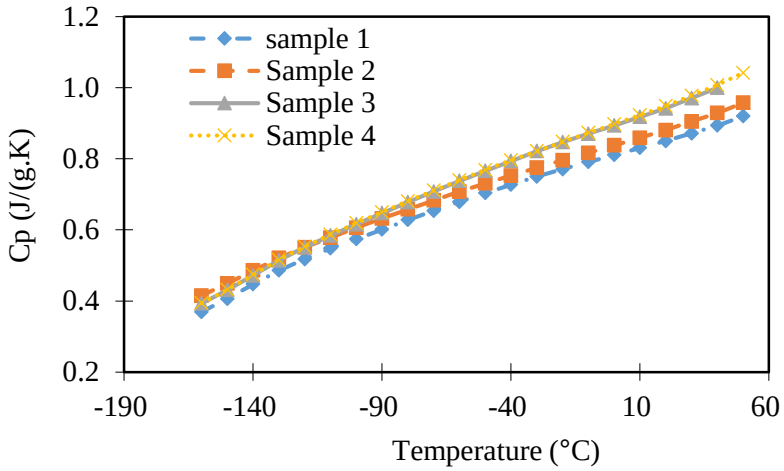

Figure 3: Specific heat capacity of powdered concrete samples using DSC

2.3 Experimental Procedure

Before starting the filling up of liquid into the concrete vaporization chamber, liquid cylinder tank is connected to a hose and the data acquisition system for the instrumented box and balance were started. The pressure build-up valve was opened to build pressure inside the liquid cylinder. Once the desired pressure was reached in the liquid tank, the liquid transfer valve was opened to transfer the liquid from the liquid tank to the vaporization chamber. In the beginning, cryogenic vapor comes out of the liquid carrying hose due to the vaporization inside the hose. After some time, liquid starts coming out of the hose. Once the liquid touches the surface of the concrete, the reading in the balance starts changing. The liquid flow to the vaporization chamber was cut well before the overflow then a relatively long time was allowed to vaporize the liquid by taking conductive heat from the concrete substrate. After a significant amount of the liquid vaporization, the chamber was replenished. The procedure was repeated 4 times for LN_2, 2 times for LO_2 and 6 times for mixtures.

3. Results and discussions

3.1 Liquid Mass Vaporization

Figure 4 shows the mass of liquid in the vaporization chamber during the course of experiments. Though it took different amount of time for liquid to reach the chamber from the liquid tank for three different types of material, in the Figure, time zero is considered when the first filling of liquid has ended. Therefore, it allows us to compare the rate of vaporization of all liquids at the beginning of the experiments. From Figure 4, at the beginning all three curves for LN_2, LO_2 and Mixture filling curve show a concave vaporization curve due to the mass loss from the conductive heat transfer from the concrete substrate. For the LN_2 experiment, the second refilling of the vaporization chamber were started at 675 second when the chamber was holding about 5 kg of liquid and the refilling ended at 764 seconds at a final liquid mass of 10.2 kg. The third re-filling started at 1772 second while the chamber was holding 3.2 kg of liquid and ended at

2008 second at 11.2 kg of liquid mass. Finally, the fourth re-filling started at 4050 second while it was holding 2.6 kg of liquid pool and ended at 4262 second at the liquid mass of 11.4 kg.
For LO_2, the second re-filling started at 1187 seconds while the chamber was holding 1.2 kg of liquid and ended at 1275 second while there were 14.6 kg of liquids. The third re-filling started at 4292 seconds while the chamber was holding 1.8 kg of LO_2 and ended at 4403 second and 13.9 kg of liquid. For the mixture of LN_2 and LO_2 of an initial composition of 80% LN_2 and 20% LO_2 in the liquid cylinder tank, the second re-filling started at 1010 second while the tank were holding 2.6 kg of liquid and ended at 1089 second with 12.5 kg of liquid. The third re-filling was started 2888 second with 2.9 kg of liquid mass and ended at 3005 second with 13.4 kg of liquid. The fourth re-filling was started at 5631 second with 3.5 kg of liquid and was ended at 5786 second with 13.4 kg of liquid. The balance used to measure the mass of the liquid has an uncertainty of ±60gm. Therefore, the maximum amount of measurement uncertainty in the data presented in Figure 4 is less than 4%.

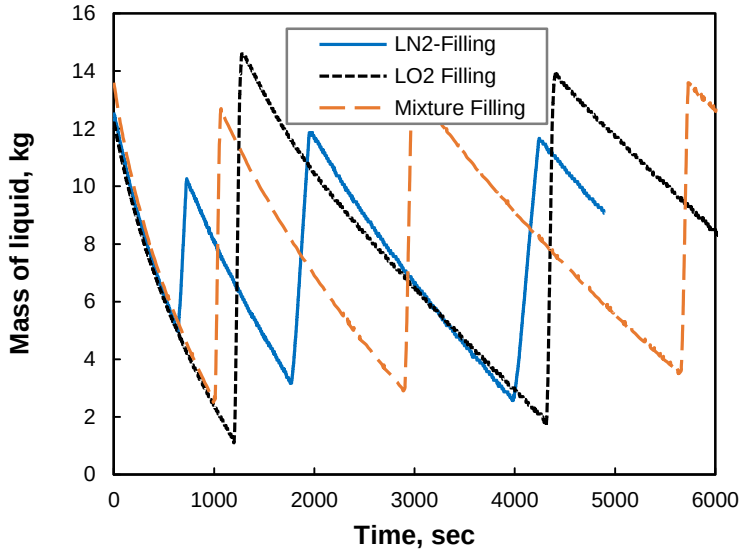

Figure 4: Mass of the liquid pool

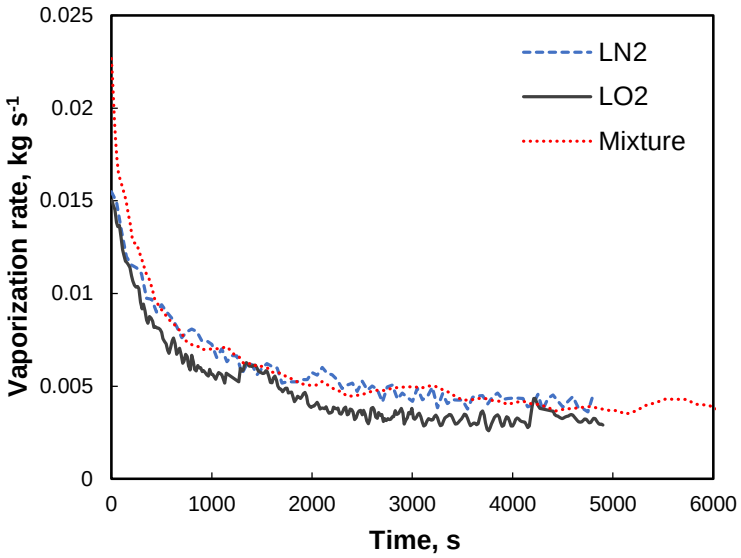

Figure 5: Mass vaporization rate of cryogenic liquids after a spill on a concrete surface

Figure 5 presents the rate of mass vaporization when cryogens were spilled in the vaporization chamber for the spill cycles presented in Figure 4. To calculate the vaporization rate, the balance data during the re-filling periods were discarded due to the fact that the estimated vaporization rate will not represent vaporization due to heat conduction only. It is clear from the Figure, the vaporization rate decreases rapidly at the beginning of the spill and tends to cease at the end of the spill. At time zero, which is considered as the end of first liquid filling in the vaporization chamber, the rate of vaporization of LN_2, LO_2 and mixture were 0.016±4%, 0.015±4% and 0.022±4% kg/s respectively. However, it would be inaccurate to draw any conclusions from this observation due to the fact that LN_2, LO_2 and mixture undergone different duration of first filling time *i.e.* 46, 44 and 30 seconds respectively. Therefore, during LN_2, and LO_2 experiments, the concrete substrate has undergone larger cooling period before time zero. The slopes of the three experiments were found to be similar from the Figure 5. At the end of the experiment, the vaporization rates of all three materials tend to be constant. At about 4800 seconds, it is observed that the steady-state vaporization rate of LN_2 (0.0045 kg/s) is higher than that of LO_2 (0.003 kg/s). The mixture vaporization rate mixture (0.004 kg/s) were found in between the steady-state vaporization rate of LN_2 and LO_2. From Figure 5, a pattern in the change of mass vaporization for LO_2 was observed at 1500 seconds. The rate of vaporization has increased from 0.005 kg/s to 0.0058 kg/s and started decreasing with a lesser negative slope. Since this phenomenon happened after the second filling of the vaporization chamber, it is difficult to conclude the exact reason of this observation. However, it could be hypothesized that either change in the boiling regime from film boiling to nucleate boiling or increase in turbulence due to the filling of the liquid in the vaporization chamber, or combination of both may cause the increase in rate.

3.2 Temperature and Heat Flux Profile inside Concrete Substrate during LN_2 Vaporization

Figure 6 depicts the transient temperature profiles inside the concrete substrate at 4 different depth layers. The initial temperature of the concrete substrate was 27.8°C before the start of spill. From Figure 6(a), it is clear that the temperature has started changing almost immediately at the thermocouples in the first layer of depth. However, from Figure 6(b), the readings of thermocouples started changing after 720 seconds of the first layer. Similarly, after 2200 seconds of spill, the temperatures of the fourth layer started changing. And for the fourth layer, it is clear from Figure 6(d) that the temperature remained same as the initial temperature of the concrete substrate. From layer 1, the rate of temperature decreases in the thermocouples which are closer to the liquid-substrate interface (*i.e.* TC-111, TC-115) are higher than the thermocouples

lies in deeper locations. Similar observations were found for the layer 2 thermocouples. Comparing the rate of change of temperatures at 5000s, layer 1 thermocouples reached to an almost steady-state condition whereas layer 2 thermocouples were changing. These observations were consistent with the 1-D heat transfer model of semi-infinite solid materials.

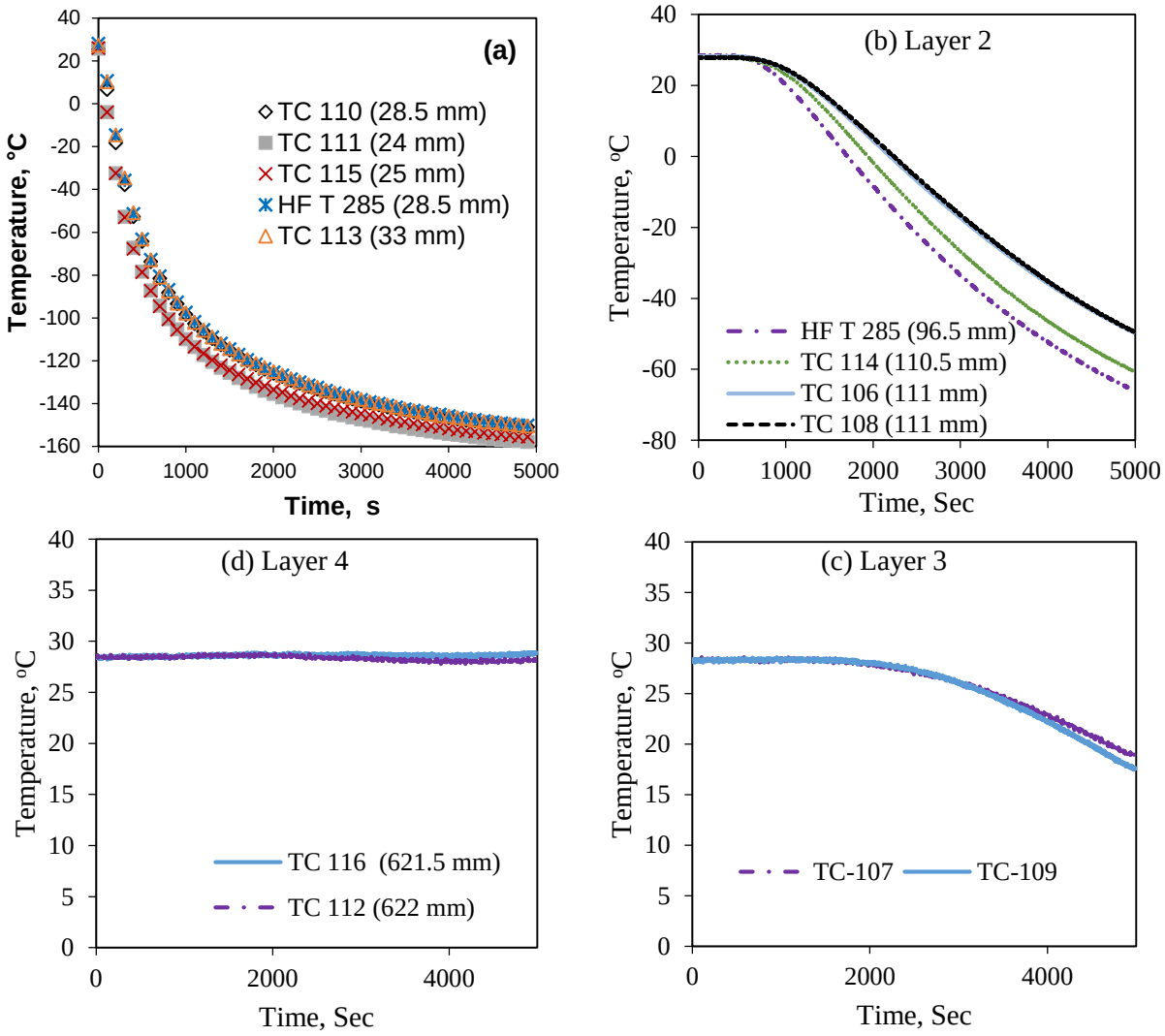

Figure 6: Temperature profile inside the concrete slab during the spill of liquid nitrogen

Figure 7 depicts the heat flux monitored at the depths of 28.5 mm (HF-X-284) and 96.5 mm (HF-X-285) inside the concrete substrate. For HF-X-284, the heat flux increased sharply and reached a maximum point and then decreases monotonically. The physical explanation of this trend is as follows. If you consider a thin slice of concrete material at the depth of the heat flux sensors, the temperature above the slice and bottom of the slice were same initially. Therefore, no heat flux was observed at the beginning. As the temperature of the top of the slice decreases due to vaporization of LN_2, a temperature gradient was created within the thin slice. The temperature gradient increases sharply causing a sharp increase of heat flux. While draining sensible heat stored within the thin slice, to vaporize the boiling liquid, results in decreasing the temperature gradient. Therefore, the heat flux decreases monotonically as the temperature gradient within the slice is decreasing. For the case HF-X-285, similar explanation can be given. However, the temperature gradient of a thin slice at the depth of heat flux sensor location was 0 for duration of 480 seconds. It took about 4000 seconds to increase the temperature gradient. Therefore, an increasing heat flux was observed

this sensor. At the end of 4000 seconds, the rate of heat flux for HF-X-285 is the same as the rate of heat flux for HF-X-284, indicating that the heat transfer rate is reaching towards a steady-state condition. Change in the observed heat fluxes from HF-X-284 and HF-X-285 sensors were compared with the estimates due to the mass vaporization as shown in Figure 5. The HF-X-284 data is not comparable to the heat flux estimation from mass vaporization because HF-X-284 does not lie at the liquid-solid interface. In addition, convective heat transfer might have small contribution in the heat flux estimates from mass vaporization. Despite heat flux from HF-X-284 agrees well with the heat flux estimation from mass vaporization data; indicating the main contributor of heat of vaporization is conduction from the substrate. Finally, the highest heat flux observed during early and steady-state conditions of LN_2 spill were 12.4 kW/m^2 and 3.7 kW/m^2.

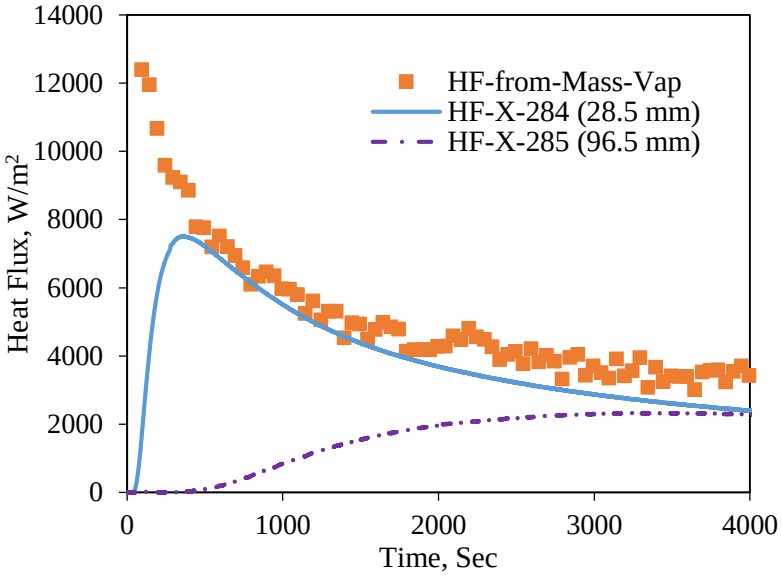

Figure 7: Heat flux to the liquid nitrogen pool

3.3 Temperature and Heat Flux Profile inside Concrete Substrate during LO_2 Vaporization

Figure 8 illustrates the temperature and heat flux profiles during the LO_2 vaporization test on the concrete substrate. The initial temperature of the concrete substrate was 32°C. It was observed that the temperature profile of the layer 3 and 4 remained constant. However, comparing to LN_2 data, no temperature change were observed in layer 3 sensors. It can be accounted to higher initial temperature (32°C) than LN_2 (27.8°C). Thus more sensible heat was stored per unit volume of concrete during the LO_2 test. Layer 1 temperature profiles show that thermocouples closer to the liquid-solid interface underwent larger temperature change than those were deeper in the concrete. From Figure 8(b), the temperature of the layer 2 thermocouples started changing at 436 seconds. Also, it validates the fact that the change in temperature is higher for thermocouples closer to the surface than the thermocouples placed deeper.

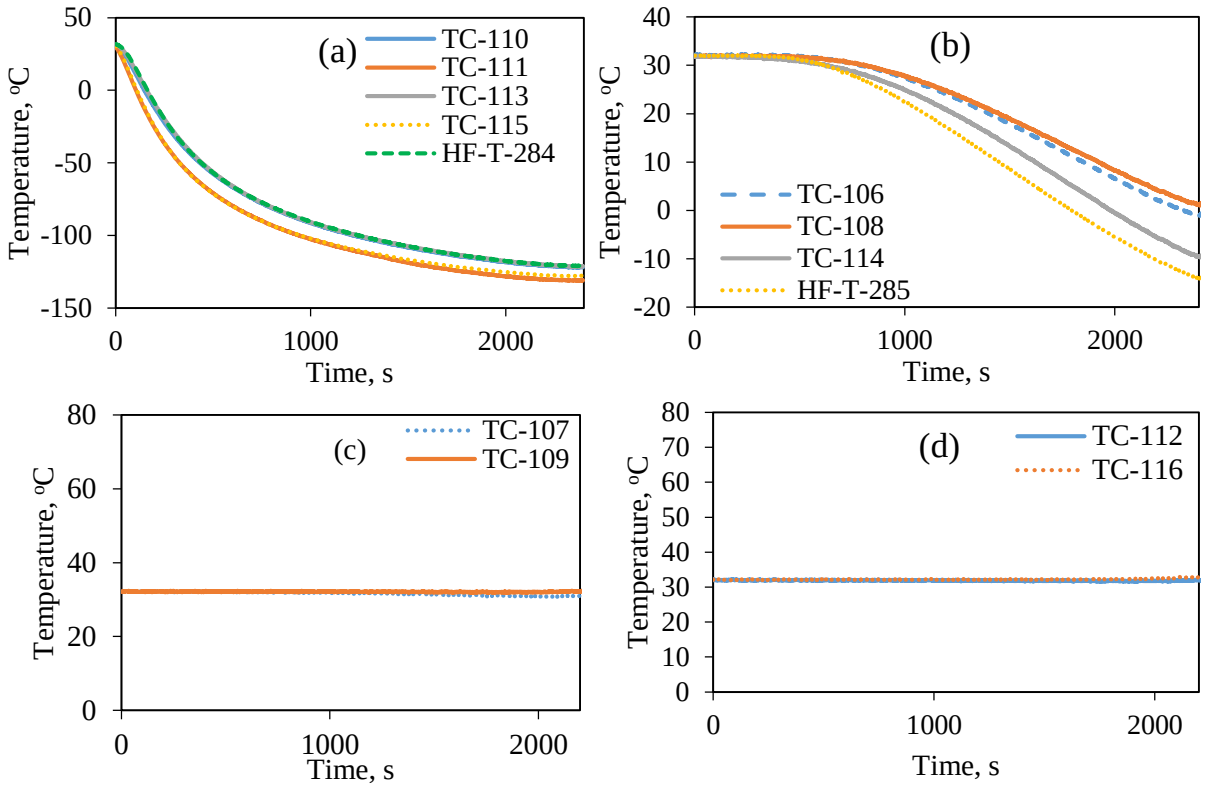

Figure 8: Temperature profile inside concrete slab during the spill of liquid oxygen.

Figure 9 shows the measured heat flux using heat flux sensors and estimates based on Figure 5 mass vaporization rates. Unlike the observations of LN_2, after the sensor data reaches the estimates, it decreases monotonically, while the estimate decreases at a higher rate. However, about time 1480 seconds, the estimated heat flux jumps over the HF-X-284 and thereafter both the sensor and estimates were in very good agreement. The phenomena of HF-X-284 sensor readings and estimates discrepancy can be explained by the mode of boiling phase change. Once the liquid boils in the film boiling regime, the rate of heat flux decreases rapidly as the vapor film between the boiling liquid and the solid substrates has low thermal conductivity. However, when the film breaks, liquid come in contact with the solid, thus the thermal resistance drops significantly and this causes an increase of heat flux. Finally, the highest heat fluxes observed during the LO_2 vaporization during early and steady-state conditions were 12.9 kW/m^2 and 2.96 kW/m^2.

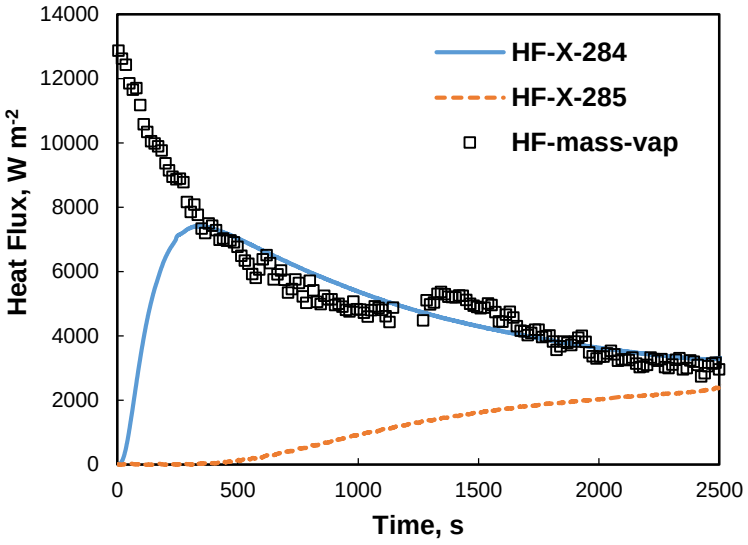

Figure 9: Conductive heat flux provided to liquid oxygen pool

3.4 Temperature and Heat Flux Profile inside Concrete Substrate during mixture vaporization

An initial mixture of 80% liquid nitrogen (LN_2) and 20% liquid oxygen (LO_2) was poured in the concrete vaporization chamber. Figure 10 presents the temperature profiles inside concrete substrate at 4 different layers. The duration of the test for mixture spill was 5.7 hours, whereas LN_2 and LO_2 were much shorter in comparison. Therefore changes in temperatures all layers of thermocouples were observed. The initial temperature of the concrete substrate was 30.3°C. At 1140 seconds, the temperature of layer 2 thermocouples started changing from the initial point. In layer 3, temperature started changing at about 2180 seconds. The temperature of the layer 4 has remained almost constant throughout the test. In Figure 10(a), a wavy pattern of temperature profiles were observed for the first layer of thermocouples at 3339, 6000, 9922 and14397 seconds. The rate of temperature change in the first layer of thermocouples was suddenly increased and then started following the decreasing trend at these time instants. This phenomenon is noticeable after the 3rd, 4th, 5th and the 6th refill of the mixture liquid in the vaporization chamber. However, the 5th and the 6th refills were not shown in Figure 4. A sudden rise in heat transfer rate at these time instants were also observed in Figure 11. This observation can be accounted due to preferential boiling of LN_2 over LO_2 during mixture vaporization. When mixture was allowed to boil in the vaporization chamber, initially LN_2 was boiling at a higher rate than the LO_2 due to its lower boiling point. As a result, just before the refill of the mixture, the concentration of LO_2 in the remaining liquid were believed to much higher than 20% of initial concentration. Once the tank was refilled with another batch of mixture liquid, the concentration of LN_2 increased. As a result, a sudden increase of heat flux which was reflected across the temperature gradient across the layer 1. At the beginning of the test, the rates of temperature and heat flux decrease were much higher to capture the subtle change due to preferential boiling. Therefore, no change in the temperature and HF-X-284 heat flux sensors data were captured in the first layer of instruments.

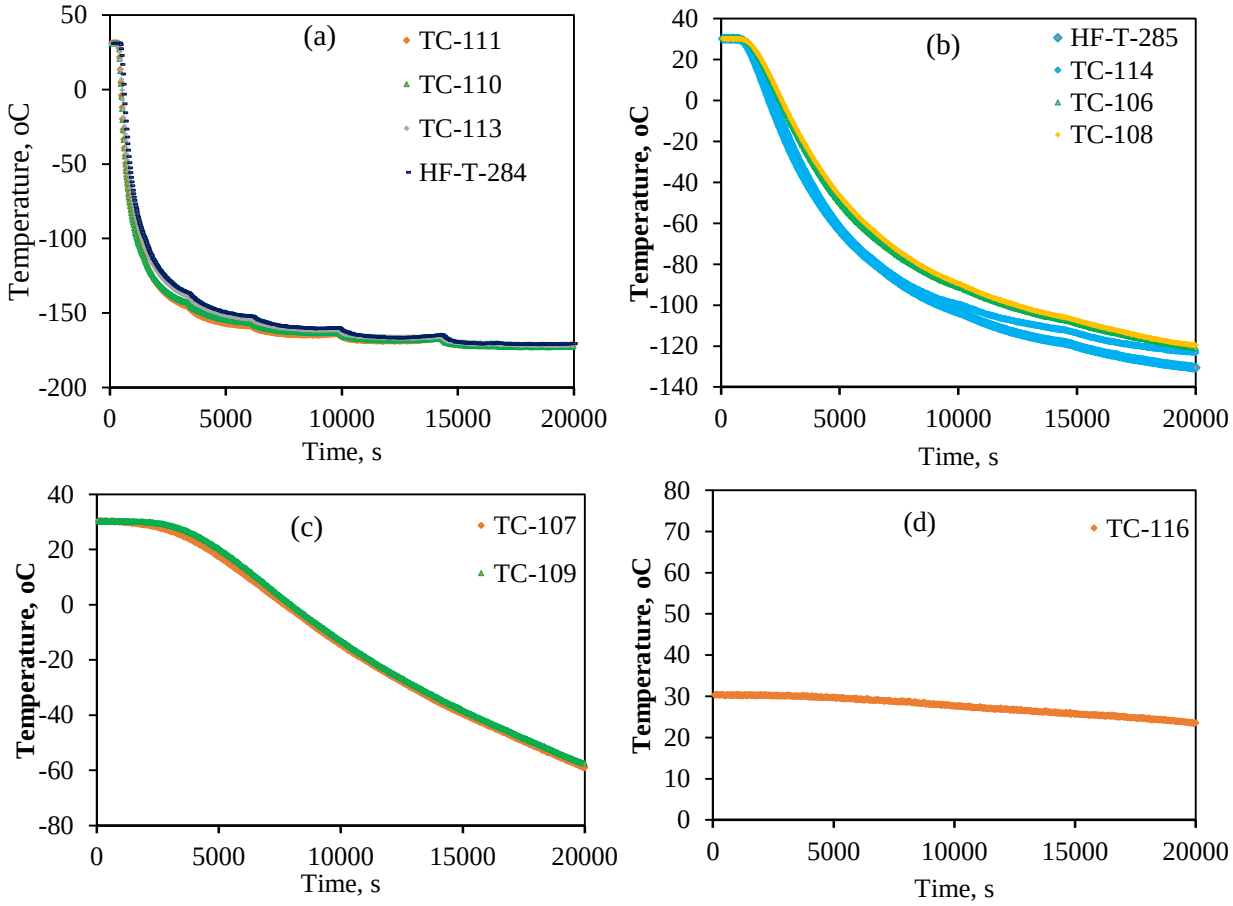

Figure 10: Temperature profile inside concrete slab during the spill of liquid nitrogen (80%) and liquid oxygen (20%) mixture.

From Figure 11, at 1100 second, there is a change in the trend of HF-X-284 reading. At the time instants of 3339 second, the change in heat flux due preferential boiling is much prominent and it resulted a 3% increase in heat flux after the refill. Subsequent observations at 6095, 9785 and 14258 seconds, the heat flux has increased by 6%, 11% and 15% after the refill of the mixture liquid to the vaporization tank. It is also shown in Figure 11 that heat fluxes from HF-X-285 overshoot that of HF-X-284 at 4294 seconds. At that instant, the temperature gradient across a thin slice of layer 1 has dropped lower than the temperature gradient across another thin slice of layer 2.

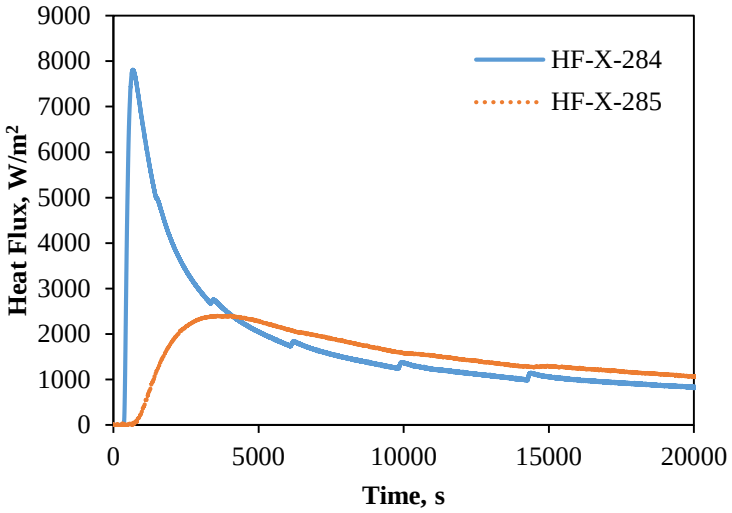

Figure 11: Heat flux inside the concrete at the depth of 28.5 mm and 96.5 mm.

3.5 Effect of mixture properties on the vaporization of cryogenic liquids

Figure 12 illustrates the temperature profiles of two first layer thermocouples (TC-110 and TC-111), two second layer of thermocouples (HF-T-285 and TC-108) and the first layer heat flux sensor (HF-X-284). It is observed from Figure 12(a) and (b) that the rate of temperature change inside the concrete substrate is higher for LN_2 in compared to LO_2 owing to lower boiling point (77K) than that of LO_2 (90K). For mixture, in the beginning, the rate of temperature change follows that of LN_2 and at the later stage it follows the trend of LO_2. From Figure 12(c), the variation among the heat flux profiles is due to the 13K wall superheat, the difference in LN_2 and LO_2 boiling points. Different rise time was observed for different material in HF-X-184 heat flux profiles. It is also seen that the slope of mixture heat flux varied from the slope of LN_2 and LO_2. In the early stage, the slope follows the trend of LN_2 and in the later stage that of LO_2.

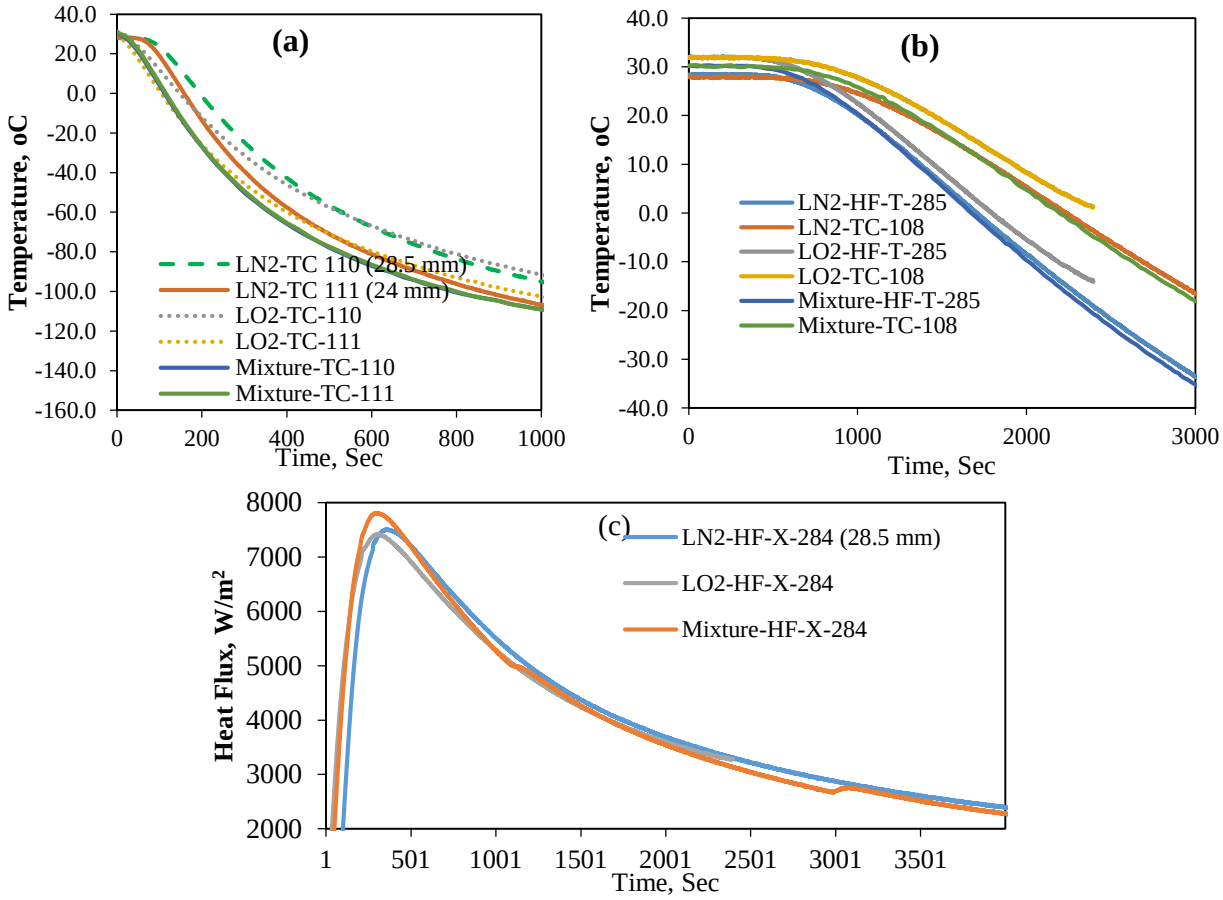

Figure 12: Effect of mixture on the temperature and heat flux profiles

4. Concluding Remarks

The concluding remarks of this study can be bulleted as follows:

- The thermal conductivity of concrete increases linearly over the temperature range of -160°C to 50°C. Within the investigated temperature range, at lower temperatures the rate of change is higher than the higher temperatures. Between -66°C to -41°C, the rate of change were found negative.
- The specific heat capacity (*Cp*) of concrete increases linearly with the increase of temperature within a range of -160°C to 50°C.
- The surface of the concrete substrate were cooled due to the vapor commence in the beginning of the each experiment. Therefore, the rate of vaporization at the very beginning of the experiment could not be estimated.
- The observations of heat flux sensors plates agree very well with the estimated heat fluxes from mass vaporization. Thus it can be concluded that the major heat transfer mechanism in the vaporization of cryogenic liquids is due to the conductive heat transfer from the concrete substrate.
- In the early stage of the spill, the highest heat flux was observed. At the later stage, the heat flux approached to a steady-state condition. The highest and the steady-state heat fluxes for LN_2 spill over a concrete substrate were recorded as 12.4 kW/m^2 and 3.7 kW/m^2. Similarly, in case of LO_2, the recorded heat fluxes were 12.9 kW/m^2 and 2.96 kW/m^2. For mixture, this could not be estimated due to the lack of knowledge of the mixture concentration at that particular moments since the mixture concentration were continuously changing due to the preferential boiling.

- The boiling phase change from film boiling to nucleate boiling has been observed during the test of LO_2. Whereas, for the LN_2 and mixture experiments, the phase change evidence is not conclusive.
- Preferential boiling of LN_2 over LO_2 was observed during the vaporization of mixture. The heat flux variations due to preferential boiling were varied from 3% to 15%. It was observed that the effect of preferential boiling is more noticeable during the later stage of pool vaporization than the earlier stage.
- The rate of temperature change during mixture vaporization follows the trend of LN_2 at the beginning and the trend of LO_2 at the later stage of the pool vaporization.

Acknowledgments

This paper was made possible by a National Priority Research Project (NPRP) award [NPRP 6-425-2-172] from the Qatar National Research Fund (a member of The Qatar Foundation). The authors sincerely acknowledge Qatar Petroleum for allowing using their facility, wind tunnel at Fire Staion-2 in Ras Laffan Industrial City (RLIC).

References

[1] D. Crowl, J.F. Louvar, Chemical Process Safety: Fundamentals with Applications, 3rd ed., Pearson Education, Boston, Massachussetts, 2011.

[2] NFPA 59A, Standard for the Production, Storage, and Handling of Liquefied Natural Gas (LNG), National Fire Protection Association, 2013.

[3] D. Burgess, M.G. Zabetakis, Fire and explosion hazards associated with liquefied natural gas, Pittsburgh, PA (USA), n.d.

[4] F. Briscoe, P. Shaw, Spread and Evaporation of Liquid, Prog. Energy Combust. Sci. 6 (1980) 127–140.

[5] T.A. Cavanaugh, J.H. Siegell, K.W. Steinberg, Simulation of Vapor Emissions From Liquid Spills, J. Hazard. Mater. 38 (1994) 41–63. doi:10.1016/0304-3894(93)E0111-E.

[6] D.M. Webber, M.J. Ivings, Modelling bund overtopping using Shallow Water Theory, J. Loss Prev. Process Ind. 23 (2010) 662–667. doi:http://dx.doi.org/10.1016/j.jlp.2010.07.002.

[7] J.L. Woodward, R. Pitblado, LNG Risk Based Safety - Modeling and Consequence Analysis, AIChE, John Wiley & Sons, Inc., Hoboken, NJ, USA; Published simultaneously in Canada, 2012.

[8] E.M. Drake, R.C. Reid, How LNG boils on soils, Hydrocarb. Process. 54 (1975).

[9] M. Ahammad, Y. Liu, T. Olewski, L. Vechot, M.S. Mannan, Application of Computational Fluid Dynamics (CFD) in Simulating Film Boiling of Cryogens, Ind. Eng. Chem. Res. (2016) acs.iecr.6b01013. doi:10.1021/acs.iecr.6b01013.

[10] R.C. Reid, R. Wang, The boiling rates of LNG on typical dike floor materials, Cryogenics (Guildf). 18 (1978) 401–404. doi:http://dx.doi.org/10.1016/0011-2275(78)90033-4.

[11] L. Véchot, T. Olewski, C. Osorio, O. Basha, Y. Liu, S. Mannan, Laboratory scale analysis of the influence of different heat transfer mechanisms on liquid nitrogen vaporization rate, J. Loss Prev. Process Ind. In Press (2012) In Press. doi:10.1016/j.jlp.2012.07.019.

[12] N. Gopalaswami, T. Olewski, L.N. Véchot, M.S. Mannan, Small-scale experimental study of vaporization flux of liquid nitrogen released on water, J. Hazard. Mater. 297 (2015) 8–16.

[13] N. Gopalaswami, L. Vechot, T. Olewski, S. Mannan, Small-scale experimental study of vaporization flux of liquid nitrogen released on ice, J. Loss Prev. Process Ind. 37 (2015) 124–131.

[14] A.J. Prince, Details and results of spill experiments of cryogenic liquids onto land and water, 1983.

[15] A.M. Thyer, A review of data on spreading and vaporisation of cryogenic liquid spills, J. Hazard. Mater. 99 (2003) 31–40. doi:10.1016/S0304-3894(02)00355-2.

[16] C. Conrado, V. Vesovic, The influence of chemical composition on vaporisation of LNG and LPG on unconfined water surfaces, Chem. Eng. Sci. 55 (2000) 4549–4562. doi:10.1016/S0009-2509(00)00110-X.